Electronic structure of the metallic ground state of $La_{2-2x}Sr_{1+2x}Mn_2O_7$ for $x \approx 0.59$ and comparison with $x = 0.36, 0.38$ compounds as revealed by angle-resolved photoemission

Z. Sun, J. F. Douglas, Q. Wang, and D. S. Dessau*
Department of Physics, University of Colorado, Boulder, Colorado 80309, USA

A. V. Fedorov
Advanced Light Source, Lawrence Berkeley National Laboratory, Berkeley, California 94720, USA

H. Lin, S. Sahrakorpi, B. Barbiellini, R. S. Markiewicz, and A. Bansil
Department of Physics, Northeastern University, Boston, Massachusetts 02115, USA

H. Zheng and J. F. Mitchell
Materials Science Division, Argonne National Laboratory, Argonne, Illinois 60439, USA
(Received 12 November 2007; revised manuscript received 29 May 2008; published 1 August 2008)

Using angle-resolved photoemission spectroscopy, we present the electronic structure of the metallic ground state of $La_{2-2x}Sr_{1+2x}Mn_2O_7$ ($x \approx 0.59$) and interpret the results in terms of first-principles band-structure computations, of which the generalized gradient approximation yields the best agreement with the experimental data. No bilayer-split bands are found in this compound, indicating the near degeneracy of electronic states in the neighboring MnO_2 layers due to its *A*-type antiferromagnetic structure. The $d_{3z^2-r^2}$ states near the zone center were not observed, which is also consistent with its *A*-type antiferromagnetic structure. Near the Fermi level, a kink in the dispersion reveals an important electron-phonon many-body interaction. The electron-phonon coupling is ~1 near the zone boundary and ~2 near the zone diagonal, showing strong *k* dependence.

DOI: 10.1103/PhysRevB.78.075101 PACS number(s): 71.18.+y, 79.60.−i, 71.20.−b, 71.27.+a

I. INTRODUCTION

In manganites, the intricate interactions of spin, charge, lattice, and orbital degrees of freedom reveal themselves in the complicated phase diagrams. Inevitably, the investigation of the electronic structure and its evolution with doping and temperature is the key to the understanding of these complex systems. Angle-resolved photoemission spectroscopy (ARPES), as a direct probe of the electronic excitations, has been playing a dominant role in the study of the electronic structures of many materials. Unlike the heavily studied perovskite $La_{1-x}Sr_xMnO_3$, $La_{2-2x}Sr_{1+2x}Mn_2O_7$ is a layered compound and its two-dimensionality makes it especially favorable for investigation using ARPES. So far, the valence-band structure of $La_{2-2x}Sr_{1+2x}Mn_2O_7$ has been clearly resolved using ARPES only at the doping levels of $x=0.36$, 0.38, and 0.4.[1–7] Recently, interest in the layered manganites at much higher doping levels has arisen. In particular, at exactly $x=0.60$ a long-range "bistripe" order sets in and the material is insulating down to the lowest temperatures. At doping levels just away from 0.60, the system is a metal at low temperature, transitions to a charge-ordered insulator at high temperatures, and finally is a paramagnetic insulator above that. Our samples had a doping level $x \approx 0.59$, with a charge order $T_c \sim 160$ K determined by the near-E_F spectral weight in ARPES—a transition temperature consistent with the samples used in Ref. 8. Although these samples of different doping levels share the same crystal structure, the complicated phase diagram indicates that their ground states are different. An investigation of the electronic structure is a good starting point for exploring the interesting physical properties of these materials.

$La_{2-2x}Sr_{1+2x}Mn_2O_7$ consists of two neighboring MnO_2 sheets alternately stacking with $(La,Sr)_2O_2$ layers along the *c* axis. In the intensively studied doping range $x \sim 0.32-0.4$, the spin ordering at low temperature is ferromagnetic both within and between the MnO_2 sheets. However, for the *A*-type antiferromagnetic $x \approx 0.59$ sample studied here, the spin arrangement is antiferromagnetic between the MnO_2 planes, but it remains ferromagnetic within the planes.[9] Through the double-exchange interaction, this is expected to lead to an almost purely two-dimensional electronic structure, which may therefore be more susceptible to fluctuations or correlation effects. Despite this two-dimensionality, the electrical conductivity of $x \approx 0.59$ samples is found to be among the greatest of all layered manganites.[8] The T_c of heavily doped layered samples is among the highest of all known bilayer manganites.

In this paper, we combine ARPES measurements and band calculations to explore the electronic structure of the metallic ground state of $La_{2-2x}Sr_{1+2x}Mn_2O_7$ ($x \approx 0.59$). In this compound, the $d_{x^2-y^2}$ states in neighboring MnO_2 layers are degenerate and the $d_{3z^2-r^2}$ states become unoccupied, consistent with its *A*-type antiferromagnetic structure. We also found that the electron-phonon many-body interaction shows a strong *k* dependence. A comparison with $x=0.36, 0.38$ samples shows that the electronic structure has a drastic change with doping in $La_{2-2x}Sr_{1+2x}Mn_2O_7$, although the crystal structure remains the same.

II. METHODOLOGY

A. Experimental details

The single crystals were grown using the traveling-solvent floating zone method as described elsewhere.[10] Rig-

orous measurements show that the ground state of this material is a metal around $x \sim 0.60$ and becomes an insulator only at perfect 60% doping.[11] The $x \approx 0.59$ samples we used here are slightly off the $x=0.60$ compound[12] and become metallic at low temperatures. In this paper, we will focus on the electronic structure of the metallic ground state of this material. All samples were cleaved and measured in an ARPES spectrometer *in situ* at $T \sim 20$ K, so that the samples were in the low-temperature ferromagnetic ($x=0.36$) or *A*-type antiferromagnetic ($x \approx 0.59$) state. The ARPES experiments were performed at Beamline 12.0.1 of the Advanced Light Source (ALS), Berkeley, using a Scienta SES100 electron analyzer under a vacuum of $\sim 2 \times 10^{-11}$ torr. The combined instrumental energy resolution was better than 20 meV, and the momentum resolution was about $0.02\pi/a$. A wide variety of polarization conditions and photon energies between 30 and 80 were used in order to optimize the photoemission matrix elements.

The surface quality of cleaved bilayer manganites is of importance for ARPES measurements. The investigation has been performed on both single-layer manganite[13] and bilayer manganite,[14] indicating that the manganite crystals cleave between the La/SrO rock-salt oxide layers, which results in a La/SrO layer on top of the first MnO_6 bilayer. These studies suggest that cleaving a layered manganite will expose a high quality surface.

B. Computational details

Detailed calculations of the electronic structure and magnetic configurations of the $x=0.5$ hole-doped double layered manganite $LaSr_2Mn_2O_7$ were performed within the all-electron full-potential Korringa-Kohn-Rostoker (KKR) and linearized augmented plane-wave (LAPW) methods.[15,16] We calculated the electronic structure of both ferromagnetic and *A*-type antiferromagnetic $LaSr_2Mn_2O_7$. The results for the ferromagnetic case are in accord with our previous studies.[17] The electronic structure for the $x=0.36$ or 0.60 compound was then obtained by using a rigid-band model in which the Fermi energy was adjusted to accommodate the correct number of electrons in the ferromagnetic or *A*-type antiferromagnetic case. Here we used the computation of 60% doping to represent the theoretical electronic structure of $x \approx 0.59$ compound and ignored the small difference in doping. Very similar results are obtained if the virtual-crystal approximation (VCA) is used to model the effects of La/Sr disorder.[18] To model exchange-correlation effects, we have considered the local spin-density approximation (LSDA), the generalized gradient approximation (GGA), and LSDA+U methods. For the LSDA+U calculations, we have used the Coulomb parameter value of U=7.2 eV suggested by Medvedeva *et al.*[19] The crystal parameters were taken from Ref. 20.

III. RESULTS AND DISCUSSION

Figure 1(a) shows the experimental Fermi-surface topology of $La_{2-2x}Sr_{1+2x}Mn_2O_7$ ($x \approx 0.59$) with only one hole pocket around the zone corners. This is strikingly different from the Fermi surface of $x=0.36/0.38$ and $x=0.4$ samples,

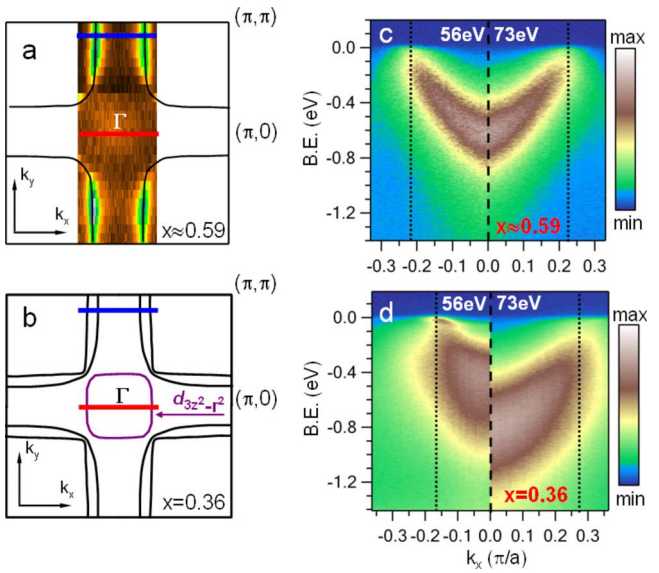

FIG. 1. (Color online) Experimental Fermi-surface topology of (a) $x \approx 0.59$ samples and (b) $x=0.36$ samples. [(c) and (d)] False color plots of spectra taken along the blue cut in (a) and (b) using 56 eV (left) and 73 (right) photons, respectively. The dotted lines indicate the momentum positions of the Fermi crossings. The temperature was 20 K, which is the low-temperature phase for both materials.

which is schematically shown in Fig. 1(b). A typical Fermi surface of $La_{2-2x}Sr_{1+2x}Mn_2O_7$ with lower doping levels (e.g., $x=0.36, 0.38, 0.40$) consists of two hole pockets around the zone corner and one additional electron pocket around the zone center.[1] The hole pockets arise primarily from in-plane $d_{x^2-y^2}$ Mn-O orbitals, which show a bilayer-split band structure, while the electron pocket is derived from the out-of-plane $d_{3z^2-r^2}$ orbitals.[1] Generally, the bilayer-split bands have different photoemission matrix elements, so that they can be selectively enhanced or suppressed by varying the photon energies and emission angles.[5,21–25] Along the blue cut in Fig. 1(a), we tuned the photoemission matrix elements by varying the incident-photon energies over a very large range from 30 to 80 eV with 3 eV step, yet we could never observe more than one band. We also searched for the bilayer-split band structure in higher Brillouin zones, but the attempts were not successful. This procedure can effectively distinguish the bilayer-split bands in $x=0.36$ and 0.38 samples, where we have found empirically that the bilayer-split individual antibonding and bonding bands can be made prominent by using 56 and 73 eV photons, respectively.[5] Figure 1(c) shows the band taken from the $x \approx 0.59$ compound along the blue cut in Fig. 1(a) using these two photon energies, but only one band is observable with $k_F \sim 0.22\pi/a$ and band bottom of ~ -600 meV. In Fig. 1(d), as a comparison, we show the bands taken from a $x=0.36$ sample under the same experimental conditions, and one can clearly see the well separated bonding and antibonding bands with different Fermi crossings ($k_F=0.17$ and $0.27\pi/a$) and band bottoms (~ -400 and -800 meV).

In two-dimensional (2-D) electronic systems such as $La_{2-2x}Sr_{1+2x}Mn_2O_7$ ($x=0.36, 0.38$) (Ref. 5) and

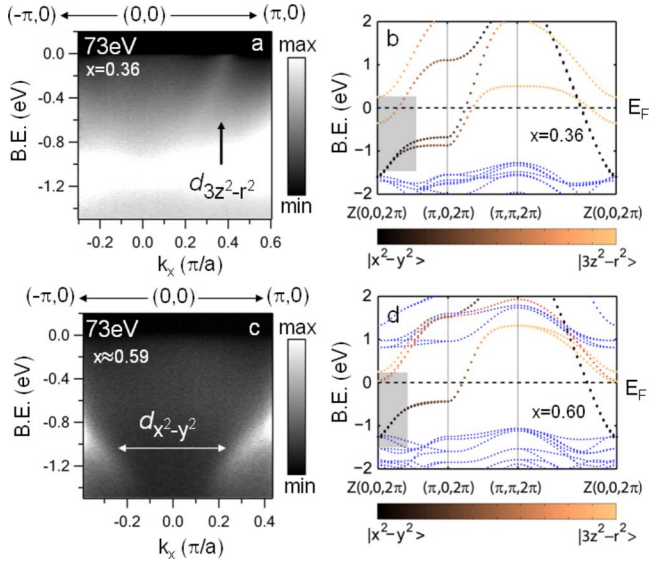

FIG. 2. (Color online) Experimental E vs k taken along the red cut in Figs. 1(a) and 1(b), showing the presence (a) or absence (c) of the $d_{3z^2-r^2}$ zone center states, depending upon doping level. Ferromagnetic and A-type antiferromagnetic GGA-based electronic band-structure calculations at the two doping levels are shown in (b) and (d), respectively, with the orbital origin of the various e_g states shown by the black/brown color scale. In (b) only the up-spin states are shown. The shadow areas in (b) and (d) indicate the positive k_x portions of (a) and (c), respectively.

$Bi_2Sr_2CaCu_2O_{8+\delta}$,[21,22] the emergence of the bilayer-split bands is due to coherent coupling along the c axis as Bloch states are formed from linear combinations of electronic orbitals in the neighboring layers. The lack of bilayer splitting in $x \approx 0.59$ is not surprising, and it is consistent with the known A-type antiferromagnetic arrangement of spins along the c axis. In particular, the double-exchange mechanism[26,27] implies that the antiferromagnetic alignment along the c axis will suppress electron hopping in the c-axis direction due to the obstruction in the spin channel.

Compared with $x=0.36, 0.38$ samples, another missing piece of the Fermi surface of $x \approx 0.59$ samples is the one corresponding to the $d_{3z^2-r^2}$ states, although some residual spectral weight can be discerned around the zone center in Fig. 1(a). Figure 2(b) shows a (ferromagnetic) GGA-based band calculation of the $x=0.36$ compound.[28,29] Comparing Figs. 2(a) and 2(b), we clearly see the presence of the $d_{3z^2-r^2}$ band in Fig. 2(a). We note here that in Fig. 2(a) the extra spectral weight near −1 eV around the zone center comes from an extra feature rather than the $d_{x^2-y^2}$ band or t_{2g} bands, with the details of this feature still under investigation. Figure 2(c) shows the spectra of $x \approx 0.59$ samples taken along the red cut in Fig. 1(a), and Fig. 2(d) shows the corresponding A-type antiferromagnetic GGA-based band calculation (for $x=0.60$). One can see that in Fig. 2(d), the calculated bottom of the $d_{3z^2-r^2}$ band and the minority t_{2g} bands are located very close to but above the Fermi energy. We also experimentally searched for the bottom of the $d_{3z^2-r^2}$ band in the $x \approx 0.59$ samples by tuning photoemission matrix elements, but it was never observed. We thus surmise that the weak spectral weight around the zone center in Fig. 1(a) probably comes from the residual weight leaking from the $d_{3z^2-r^2}$ band or the minority t_{2g} bands above the Fermi level. In fact, the $d_{3z^2-r^2}$ states dominate the hopping of e_g electrons along the c-axis direction, so their absence below the Fermi level is consistent with the A-type antiferromagnetism in $x \approx 0.59$ samples.

Notably, for $x=0.60$, the GGA-based band calculation, shown in Fig. 2(d), supports the experimental observations that only the $d_{x^2-y^2}$ bands cross the Fermi level and the bilayer splitting is very small—its theoretical value ranges from 0 meV to a maximum of 20 meV. In the zone-boundary regions, the theoretical splitting is 0 meV near the Fermi level, consistent with our experimental observation. Band calculations show the largest splitting of 20 meV at $(0.75\pi, 0)$. At that position, the measured linewidths are of a few hundred meV, and so the splitting, if it existed, would be nearly impossible to resolve. Band calculations also give a theoretical splitting of 15 meV near the zone-diagonal regions, which future ultraresolution work may potentially be able to resolve. Here we emphasize that the splittings of the lowest bands below E_F around $(\pi, 0)$ for the ferromagnetic phase in Fig. 2(b) as well as for the antiferromagnetic phase in Fig. 2(d) are of a different origin. In the ferromagnetic phase, all MnO_2 layers are identical and the associated orbitals possess the same on-site energies. The splitting of two identical orbitals in this case is due primarily to the nearest-neighbor hopping between two adjacent MnO_2 layers. In the antiferromagnetic phase, on the other hand, the two MnO_2 layers possess opposite spins and their on-site energies are different due to the exchange splitting. One of the spin-split bands is then lifted above the Fermi level. The extremely small bilayer splitting comes about due to the small hopping amplitude between the identically spin-aligned next-nearest-neighbor MnO_2 layers.

It is interesting that in contrast to the GGA scheme, the LSDA theory predicts a small minority Fermi-surface pocket of d_{xy} character for $x \approx 0.59$, which is not consistent with the experimental data. The reason for this difference between LSDA and GGA is that the exchange splitting within the LSDA is about 3 eV compared to the GGA value of 3.5 eV. The LSDA+U approximation is in even poorer agreement with experiments as follows: (1) It predicts a huge exchange splitting of 8 eV. (2) It pushes the $d_{3z^2-r^2}$ level high above the Fermi level (about 0.3 eV), which is too high to explain the remnant spectral weight around the zone center (assuming that it is due to the leaking from states above the Fermi level). (3) It pushes a filled apical oxygen band within 1 eV below the Fermi level at the Γ point, where it should have been observed in the experiment. (4) Contrary to the experimental observations, an LSDA+U calculation for lightly doped ferromagnetic phase ($x=0.36$) predicts a small bilayer splitting (~35 meV). We conclude that in $La_{2-2x}Sr_{1+2x}Mn_2O_7$ the GGA approximation seems to capture the exchange-correlation physics better than LSDA or LSDA+U approximations. The GGA provides a simple but potentially accurate step beyond LSDA, which includes the effect of the density gradient in the exchange-correlation functional. It has been shown[30] that the spin-polarized version of the GGA usually yields larger exchange splittings than the LSDA for the same geometry. In the present case,

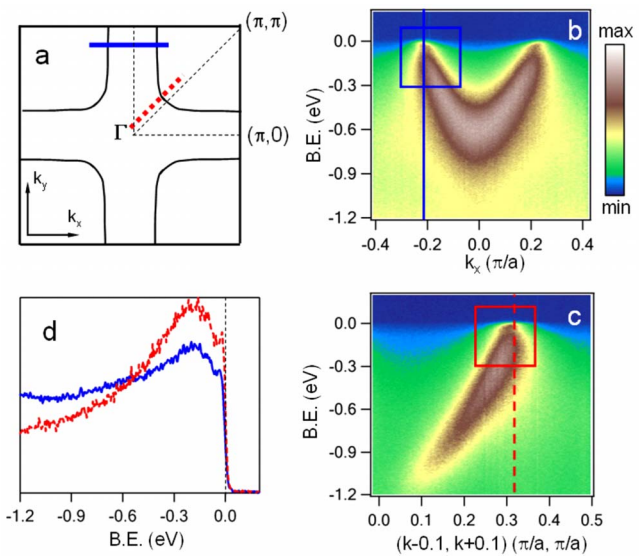

FIG. 3. (Color online) (a) A schematic Fermi-surface plot of $x \approx 0.59$ samples. [(b) and (c)] Energy vs momentum dispersive band taken along the blue and red cuts in (a), respectively. 56 eV photons were used to take these spectra. (d) EDCs taken at the Fermi crossings in (b) and (c), with the color labeling maintained.

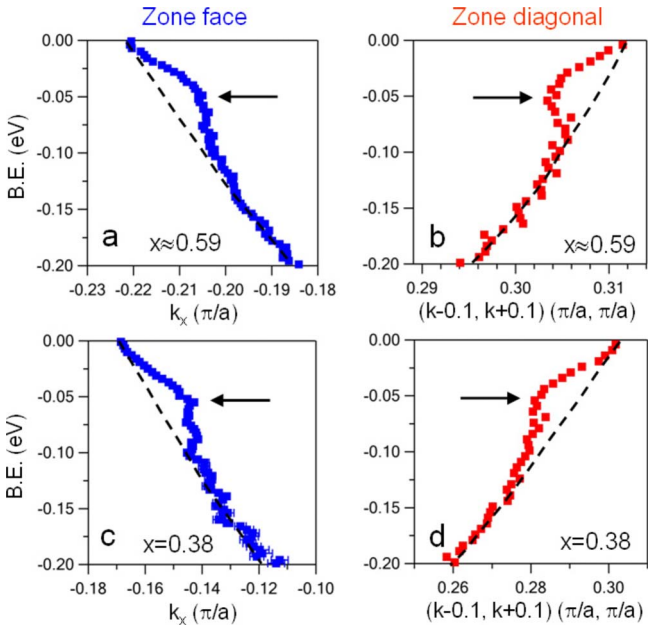

FIG. 4. (Color online) [(a) and (b)] Band dispersions of $x \approx 0.59$ samples within the blue and red frames in Figs. 3(b) and 3(c), respectively, determined by fitting MDCs with Lorentzian line shapes. [(c) and (d)] Band dispersions of antibonding $d_{x^2-y^2}$ states of $x=0.38$ samples taken at similar positions to the ones in (a) and (b). The dashed lines indicate the noninteracting (relative to phonons) dispersions.

the GGA tendency to favor magnetic properties gives good results, while the corrections by the LSDA+U scheme are clearly exaggerated.

Similar to other doping levels of $La_{2-2x}Sr_{1+2x}Mn_2O_7$, the Fermi surface is nested near the zone boundary.[3,5] Here we have a measured nesting vector $q \sim 0.22(2\pi/a, 0)$, which is two times of $k_F \sim 0.22\pi/a$, and is in agreement (within experimental momentum resolution) with the theoretically predicted value of $k_F = 0.21\pi/a$ for $x=0.60$ compound. Additionally, the hole doping determined by the Fermi-surface volume in Fig. 1(a) is ~0.6, highly consistent with the doping concentration of the sample. The magnitude of the nesting vector is also in good agreement with the bulk determination of a superlattice bistripe-type charge-ordering vector (0.21, 0.21, 0).[8] The agreement between the Fermi-surface nesting vectors and the superlattice charge-ordering vectors is not a mere coincidence, and it indicates a close connection between the Fermi surface in k space and charge ordering in real space. We will further discuss this interesting correlation in a future paper. Indeed, the agreement between ARPES measurements and theoretical calculations as well as charge-ordering vectors helps to confirm the bulklike nature of the electronic structure probed in the ARPES experiments.

Figure 3(a) is a schematic plot of the Fermi surface of $x \approx 0.59$ samples. Near the zone boundary (blue line) and diagonal cut (red line), we measured the dispersive $d_{x^2-y^2}$ band at $T=17$ K, as shown in Figs. 3(b) and 3(c). Figure 3(d) shows the energy distribution curves (EDCs) taken at the Fermi crossings (dashed line) in Figs. 3(b) and 3(c). Both of them display a quasiparticlelike peak and a large spectral weight at the Fermi level, characterizing the good metallicity of this material. This is in accord with the resistivity measurements, in which this material shows the best conductance among metallic bilayer manganites.[8]

By fitting the momentum distribution curves (MDCs) with a Lorentzian line shape on top of a small monotonically varying background, we can determine the near-E_F dispersion relation within the blue frame in Fig. 3(b), which shows a "kink" around 50–60 meV [see arrow in Fig. 4(a)]. As discussed in detail in our earlier study of the $x=0.36$ and 0.38 compounds,[5] this behavior indicates the coupling of the near-Fermi electrons to a bosonic excitation, with the energy and momentum scales of the boson related to the kink energy and the nesting vector, respectively. Overlaying the energy (50–60 meV) and momentum scale $[0.22(2\pi/a)]$ in Fig. 2(d) of Ref. 5, we see that the current kink seems to agree well with coupling to both the bond-bending and bond-stretching phonons of $x=0.4$ samples, though there as yet have been no actual phonon measurements made on samples with compositions near $x=0.6$. We also obtained the dispersion relation along the red cut in Fig. 3(a), which is shown in Fig. 4(b) with a kink near ~50–60 meV.

The strength of the electron-boson coupling is related to the strength of the kink, which can be parameterized by the ratio of the slopes of the low-energy (near-E_F) renormalized dispersion and the bare or noninteracting (relative to phonons) dispersion. The latter is indicated by the dashed line in Figs. 4(a) and 4(b). In a simple electron-boson coupling model, this ratio is $1/(1+\lambda)$, where λ is a measure of the electron-boson coupling strength. Since the ratio of these slopes is ~1/2 in Fig. 4(a), we estimate the electron-boson coupling strength at low temperature is ~1, near the zone boundary, similar to the value in $x=0.38$ samples.[5] In Fig. 4(b), the ratio of the slopes is ~1/3, which gives a coupling strength of ~2, larger than the one near the zone boundary. In contrast, the electron-phonon coupling strength has minimal changes throughout the Fermi surface in $x=0.38$

samples. In Figs. 4(c) and 4(d), we show the dispersions of the antibonding $d_{x^2-y^2}$ states of $x=0.38$ samples taken from the same momentum positions and using the same experimental parameters as those in Figs. 4(a) and 4(b), respectively. They clearly show similar electron-phonon coupling strength of ~ 1 near the zone boundary and near the zone-diagonal cut. The drastic change in the electron-phonon coupling strength in $x \approx 0.59$ samples may suggest strong k-dependent transport properties in this 2-D material. How this anisotropy happens is not clear, and further study is needed to uncover its origin and its influence on the carrier transport.

The study of the A-type antiferromagnetic phase is still under way, and only a small body of information is available, in contrast to the intensively studied ferromagnetic phase. More investigations are demanded to explore the nature of the A-type antiferromagnetic phase, in particular the physical properties near $x=0.60$, where the metallic states compete strongly with the bistripe charge/orbital ordering.

IV. CONCLUSION

In summary, we have presented the electronic structure of the metallic ground state of $La_{2-2x}Sr_{1+2x}Mn_2O_7$ ($x \approx 0.59$) and interpreted the results in terms of the corresponding GGA-based band-structure computations. We found that, due to the A-type antiferromagnetic spin ordering, there is no bilayer-split band structure and the $d_{3z^2-r^2}$ states are unoccupied. A kink structure in the dispersion relation is observed, suggesting strong electron-phonon coupling with $\lambda \sim 1-2$. Strong momentum dependence of may indicate anisotropic transport properties in $x \approx 0.59$ samples.

ACKNOWLEDGMENTS

Primary support for this work was from the U.S. National Science Foundation under Grant No. DMR 0706657, with supplementary support from the U.S. Department of Energy under Grant No. DE-FG02–03ER46066. The Advanced Light Source is supported by the Director, Office of Science, Office of Basic Energy Sciences, of the U.S. Department of Energy under Contract No. DE-AC02–05CH11231. The theoretical work was supported by the U.S. Department of Energy Contracts No. DE-FG02-07ER46352 and No. DE-AC03-76SF00098 and benefited from the allocation of supercomputer time at the NERSC and the Northeastern University's Advanced Scientific Computation Center (ASCC). Argonne National Laboratory, a U.S. Department of Energy Office of Science Laboratory, is operated under Contract No. DE-AC02-06CH11357.

*dessau@colorado.edu

[1] D. S. Dessau, T. Saitoh, C.-H. Park, Z.-X. Shen, P. Villella, N. Hamada, Y. Moritomo, and Y. Tokura, Phys. Rev. Lett. **81**, 192 (1998).

[2] T. Saitoh, D. S. Dessau, Y. Moritomo, T. Kimura, Y. Tokura, and N. Hamada, Phys. Rev. B **62**, 1039 (2000).

[3] Y.-D. Chuang, A. D. Gromko, D. S. Dessau, T. Kimura, and Y. Tokura, Science **292**, 1509 (2001).

[4] N. Mannella, W. L. Yang, X. J. Zhou, H. Zheng, J. F. Mitchell, J. Zaanen, T. P. Devereaux, N. Nagaosa, Z. Hussain, and Z.-X. Shen, Nature (London) **438**, 474 (2005).

[5] Z. Sun, Y.-D. Chuang, A. V. Fedorov, J. F. Douglas, D. Reznik, F. Weber, N. Aliouane, D. N. Argyriou, H. Zheng, J. F. Mitchell, T. Kimura, Y. Tokura, A. Revcolevschi, and D. S. Dessau, Phys. Rev. Lett. **97**, 056401 (2006).

[6] Z. Sun, J. F. Douglas, A. V. Fedorov, Y.-D. Chuang, H. Zheng, J. F. Mitchell, and D. S. Dessau, Nat. Phys. **3**, 248 (2007).

[7] S. de Jong, Y. Huang, I. Santoso, F. Massee, W. K. Siu, A. Mans, R. Follath, O. Schwartzkopf, and M. S. Golden, arXiv:cond-mat/0611287 (unpublished).

[8] Q. A. Li, K. E. Gray, S. N. Ancona, H. Zheng, S. Rosenkranz, R. Osborn, and J. F. Mitchell, Phys. Rev. Lett. **96**, 087201 (2006).

[9] J. F. Mitchell, D. N. Argyriou, A. Berger, K. E. Gray, R. Osborn, and U. Welp, J. Phys. Chem. B **105**, 10731 (2001).

[10] J. F. Mitchell, D. N. Argyriou, J. D. Jorgensen, D. G. Hinks, C. D. Potter, and S. D. Bader, Phys. Rev. B **55**, 63 (1997).

[11] K. Gray, H. Zheng, Qing'An Li, J. F. Mitchell, S. N. Ancona, S. Rosenkranz, and R. Osborn, APS March Meeting, 2007 (unpublished).

[12] We note here that the $x \sim 0.6$ sample in Ref. 8 and in these studies were all provided by the same sample grower. Our ARPES data show a metal-insulator transition at $T_c \sim 160$ K, which is in excellent agreement with the transport data of Ref. 8. According to Ref. 11, the samples used in Ref. 8 had a doping $x \approx 0.59$ or 0.61 and the metal-insulator transition temperatures is symmetric with respect to $x \approx 0.60$. We therefore can estimate that our samples are either $x \approx 0.59$ or $x \approx 0.61$. In order to determine the doping of samples we used here, we selected $x \approx 0.61$ compounds from a batch of samples. Using $x \approx 0.61$ compounds as a reference, we spectroscopically found that the samples we used here possessed larger Fermi crossings and deeper band bottoms, indicative of a lower doping, i.e. $x \approx 0.59$.

[13] Y. Wakabayashi, M. H. Upton, S. Grenier, J. P. Hill, C. S. Nelson, H. Zheng, and J. F. Mitchell, Thin Solid Films **515**, 5741 (2007).

[14] F. Loviat, H. M. Rønnow, Ch. Renner, G. Aeppli, T. Kimura, and Y. Tokura, Nanotechnology **18**, 044020 (2007).

[15] A. Bansil, S. Kaprzyk, P. E. Mijnarends, and J. Tobola, Phys. Rev. B **60**, 13396 (1999).

[16] P. Blaha, K. Schwarz, G. K. H. Madsen, D. Kvasnicka, and J. Luitz, *WIEN2k, An Augmented Plane Wave Plus Local Orbitals Program for Calculating Crystal Properties* (Karlheinz Schwarz, Technische Universität Wien, Austria, 2001).

[17] P. E. Mijnarends, S. Kaprzyk, B. Barbiellini, Yinwan Li, J. F. Mitchell, P. A. Montano, and A. Bansil, Phys. Rev. B **75**, 014428 (2007).

[18] H. Lin, S. Sahrakorpi, R. S. Markiewicz, and A. Bansil, Phys. Rev. Lett. **96**, 097001 (2006).

[19] J. E. Medvedeva, V. I. Anisimov, M. A. Korotin, O. N. Mryasov, and A. J. Freeman, J. Magn. Magn. Mater. **237**, 47 (2001).
[20] R. Seshadri, A. Maignan, M. Hervieu, N. Nguyen, and B. Raveau, Solid State Commun. **101**, 453 (1997).
[21] Y. D. Chuang, A. D. Gromko, A. Fedorov, Y. Aiura, K. Oka, Yoichi Ando, H. Eisaki, S. I. Uchida, and D. S. Dessau, Phys. Rev. Lett. **87**, 117002 (2001).
[22] D. L. Feng, N. P. Armitage, D. H. Lu, A. Damascelli, J. P. Hu, P. Bogdanov, A. Lanzara, F. Ronning, K. M. Shen, H. Eisaki, C. Kim, J.-i. Shimoyama, K. Kishio, and Z. X. Shen, Phys. Rev. Lett. **86**, 5550 (2001).
[23] A. Bansil and M. Lindroos, Phys. Rev. Lett. **83**, 5154 (1999).
[24] Y.-D. Chuang, A. D. Gromko, A. V. Fedorov, Y. Aiura, K. Oka, Yoichi Ando, M. Lindroos, R. S. Markiewicz, A. Bansil, and D. S. Dessau, Phys. Rev. B **69**, 094515 (2004).
[25] A. A. Kordyuk, S. V. Borisenko, T. K. Kim, K. A. Nenkov, M. Knupfer, J. Fink, M. S. Golden, H. Berger, and R. Follath, Phys. Rev. Lett. **89**, 077003 (2002).
[26] P. W. Anderson and H. Hasegawa, Phys. Rev. **100**, 675 (1955).
[27] K. Kubo, J. Phys. Soc. Jpn. **33**, 929 (1972).
[28] Here we show only the band calculation of the spin-up states because all major bands below the Fermi level are made up of these majority states. The GGA-based band-structure calculations for spin-down states were also performed, showing a small Fermi surface of t_{2g} minority states around Γ point, similar to those in Ref. 29.
[29] P. K. de Boer and R. A. de Groot, Phys. Rev. B **60**, 10758 (1999).
[30] B. Barbiellini, E. G. Moroni, and T. Jarlborg, J. Phys.: Condens. Matter **2**, 7597 (1990).